Biochem. J. (2012) **441**, 317–323 (Printed in Great Britain) doi:10.1042/BJ20111617

Domain assembly of NAADP-gated two-pore channels

Dev CHURAMANI*[1], Robert HOOPER*[1], Eugen BRAILOIU† and Sandip PATEL*[2]

*Department of Cell and Developmental Biology, University College London, London WC1E 6BT, U.K., and †Department of Pharmacology, Temple University School of Medicine, Philadelphia, PA 19140, U.S.A.

TPCs (two-pore channels) have recently been identified as targets for the Ca^{2+}-mobilizing messenger NAADP (nicotinic acid–adenine dinucleotide phosphate). TPCs have a unique structure consisting of cytosolic termini, two hydrophobic domains (I and II) each comprising six transmembrane regions and a pore, and a connecting cytosolic loop; however, little is known concerning how these channels are assembled. In the present paper, we report that both domain I and II of human TPCs are capable of independent insertion into membranes, whereas the loop linking the domains fails to insert. Pairs of transmembrane regions within domain I of TPC1 are also capable of insertion, consistent with sequential translational integration of hydrophobic regions. Insertion of the first two transmembrane regions, however, was inefficient, indicating possible interaction between transmembrane regions during translation. Both domains, and each pair of transmembrane regions within domain I, were capable of forming oligomers, highlighting marked redundancy in the molecular determinants driving oligomer formation. Each hydrophobic domain formed dimers upon cross-linking. The first four transmembrane regions of TPC1 also formed dimers, whereas transmembrane regions 5 and 6, encompassing the pore loop, formed both dimers and tetramers. TPCs thus probably assemble as dimers through differential interactions between transmembrane regions. The present study provides new molecular insight into the membrane insertion and oligomerization of TPCs.

Key words: calcium signalling, domain assembly, nicotinic acid–adenine dinucleotide phosphate (NAADP), two-pore channel (TPC), voltage-gated ion channel.

INTRODUCTION

NAADP (nicotinic acid–adenine dinucleotide phosphate) is a potent Ca^{2+}-mobilizing messenger, active in a wide variety of cells [1–4]. It is produced in response to a number of extracellular cues including hormones such as cholecystokinin [5] and neurotransmitters such as glutamate [6] (reviewed in [7]). NAADP-evoked Ca^{2+} signals have been implicated in many Ca^{2+}-dependent processes ranging from fertilization [8,9] to blood pressure control [10] (reviewed in [11]). Antagonizing NAADP action has recently been shown to reduce symptoms of autoimmune encephalomyelitis [12]. In a multitude of cells, NAADP appears to mobilize Ca^{2+} from acidic organelles [13], such as lysosomes [5], secretory vesicles [14] and endosomes [15], the so-called 'acidic Ca^{2+} stores' [16,17]. These signals are often amplified by archetypal Ca^{2+} channels (inositol trisphosphate and ryanodine receptors) on the ER (endoplasmic reticulum) [18]. NAADP is thus thought to trigger complex Ca^{2+} signals [4]. However, other lines of evidence suggest that NAADP mobilizes Ca^{2+} from the ER through direct activation of ryanodine receptors [19,20] or stimulates Ca^{2+} influx [21,22]. Thus, despite its established physiological and likely pathophysiological importance, the molecular basis for Ca^{2+} release by NAADP is not entirely clear [23].

Of note are a series of reports from independent laboratories that have converged on the TPCs (two-pore channels) as likely NAADP targets responsible for the mobilization of Ca^{2+} from acidic organelles [24–26]. Three isoforms (TPC1–TPC3) are present in sea urchins [27,28] (where the effects of NAADP were discovered [29]), but there has been striking lineage-specific loss of TPC3 in certain mammals, including humans [27,30]. TPCs localize to the endolysosomal system and enhance NAADP-evoked Ca^{2+} signals when overexpressed [24–28,31–33]. Knockdown of TPCs [24,25,33] or overexpression of TPCs harbouring a point mutation within the putative pore [24,32,33] inhibit endogenous NAADP responses. NAADP-evoked Ca^{2+} signals mediated by TPCs are amplified by ER Ca^{2+} channels [24,25], but only when TPCs are correctly targeted to the endolysosomal system through an identified targeting motif [34]. Biophysical analyses indicate that TPCs are NAADP-gated Ca^{2+}-permeable pore-forming subunits [34–36]. Physiological roles for TPCs have been confirmed in smooth muscle contraction [37], differentiation [38] and endothelial cell activation [39], processes in which NAADP-evoked Ca^{2+} signals had previously been implicated [10,40,41]. Additional unanticipated roles for TPCs have been identified in endolysosomal trafficking [28] and autophagy [32]. Thus multiple lines of evidence (reviewed in [7,42]) point to this poorly characterized family of ion channels as the long sought NAADP target, important for Ca^{2+}-dependent function.

At this early stage, little is known concerning the molecular architecture of TPCs. TPCs are members of the superfamily of voltage-gated ion channels [43]. They are structurally unusual in that they contain two homologous hydrophobic domains (I and II) each comprising six TM (transmembrane) regions and a pore (Figure 1) connected by a cytosolic loop. This contrasts with voltage-sensitive K^+ channels and TRP (transient receptor potential) channels which contain one such domain, and voltage-sensitive Na^+/Ca^{2+} channels which contain four [43]. The basic topology of TPCs has recently been defined [44] using a combination of fluorescence protease protection assays, antibody epitope mapping and N-glycosylation analysis. In the present study, we address membrane insertion and oligomerization of TPCs.

Abbreviations used: BS^3, bis(sulfosuccinimidyl) suberate; ER, endoplasmic reticulum; GFP, green fluorescent protein; HEK, human embryonic kidney; NAADP, nicotinic acid–adenine dinucleotide phosphate; PNGase F, peptide N-glycosidase F; TM, transmembrane; TPC, two-pore channel; TRP, transient receptor potential.

[1] These authors contributed equally to this work.

[2] To whom correspondence should be addressed (email patel.s@ucl.ac.uk).

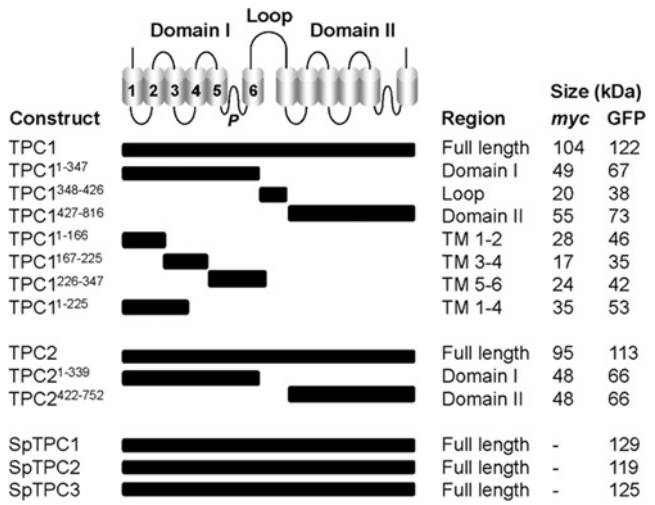

Figure 1 Dissecting the domain architecture of TPCs

Top panel: schematic illustration of the TPC showing the two hydrophobic domains (I and II) each comprising six TM regions (numbered in domain I) and a pore (*P*). The domains are connected by a cytosolic loop. A summary of the constructs used in the present study encoding the indicated region, together with the predicted size of the Myc- and/or GFP-fusion proteins are listed in the bottom part of the Figure. Constructs correspond to human (TPC1 and TPC2) or sea urchin (SpTPC1–3) isoforms.

MATERIALS AND METHODS

Plasmids

Constructs (in pCS2 +) encoding full-length human TPC1 and TPC2 tagged at their C-termini with five Myc tags (TPC1–Myc and TPC2–Myc) or GFP (green fluorescent protein; TPC1–GFP and TPC2–GFP) have been described previously [24,45]. Constructs (also in pCS2 +) encoding full-length sea urchin TPC1, TPC2 and TPC3 tagged at their C-termini with GFP (SpTPC1–GFP, SpTPC2–GFP and SpTPC3–GFP) have been described previously [27]. Constructs encoding C-terminally Myc-tagged human TPC1 fragments schematically depicted in Figure 1 were generated by PCR using IMAGE clone 40148827 (accession number BC150203) or pCS2 + TPC1 L273P, described in [24] for TPC1$^{226–347}$, as a template. The primers used are listed in Supplementary Table S1 (at http://www.BiochemJ.org/bj/441/bj4410317add.htm). The products were digested with ClaI/EcoRI and ligated together with the EcoRI/XbaI fragment from pCS2 + TPC1–Myc (encompassing the five Myc tags) into the ClaI and XbaI sites of pCS2 +. Constructs encoding C-terminally GFP-tagged TPC1 fragments were generated by cloning the ClaI/EcoRI-digested PCR products directly into the corresponding sites of pCS2 + TPC1–GFP [24]. A construct encoding C-terminally Myc-tagged domain I of TPC2 was generated by replacing the Xho and XbaI fragment of pCS2 + TPC2$^{1–339}$–GFP (encoding the GFP tag) [44] with the corresponding region of pCS2 + TPC2–Myc harbouring the five Myc tags. Constructs encoding C-terminally Myc- and GFP-tagged domain II of TPC2 were generated by PCR using IMAGE clone 5214862 (accession number BC063008) as a template and the primers listed in Supplementary Table S1. The products were cloned into the EcoRI and XhoI sites of pCS2 + TPC2–Myc or pCS2 + TPC2–GFP. The coding sequences of all plasmids were fully sequenced.

Cell culture and transfection

HEK (human embryonic kidney)-293 cells were cultured and plated as described previously [24]. They were transiently transfected with plasmids using Lipofectamine™ 2000 transfection reagent (Invitrogen) according to the manufacturer's instructions. Cells were harvested 1 day after transfection by scraping, washed once in PBS by centrifugation (500 ***g*** for 5 min) and resuspended in the indicated buffer (10 μl/cm^2 adherent cells).

Subcellular fractionation

HEK-293 cells expressing the specified Myc-tagged constructs were resuspended in intracellular-like buffer composed of 110 mM potassium acetate, 2 mM $MgCl_2$ and 20 mM sodium Hepes (pH 7.2). Samples (100 μl) were sonicated (1×5 s burst), centrifuged for 10 min at 4 °C at 1000 ***g*** (to remove debris and nuclei) and the supernatant was recovered and diluted either in an equal volume of intracellular-like buffer or 0.2 M Na_2CO_3 (pH 11). Samples were incubated at 4 °C for 60 min and centrifuged (90 000 ***g*** for 60 min at 4 °C). The supernatant was recovered and the resulting pellet was resuspended into the original volume of the appropriate buffer. Aliquots (typically 10 μl) were subject to SDS/PAGE followed by Western blot analysis.

Preparation of detergent-solubilized cell homogenates

HEK-293 cells expressing the indicated Myc- and/or GFP-tagged construct(s) were resuspended in solubilization buffer comprising 20 mM Tris/HCl (pH 7.2), 50 mM NaCl, 10 mM magnesium acetate, 1 % Triton X-100 (Pierce) and an EDTA-free protease inhibitor mixture (Roche). The suspension was rotated for 60 min at 4 °C, centrifuged (90 000 ***g*** for 60 min at 4 °C) and the supernatant was recovered.

Co-immunoprecipitation

Detergent-solubilized cell homogenates (200 μl) were incubated overnight at 4 °C with 2.5 μg of anti-Myc antibody (9e10, Santa Cruz Biotechnology) on a rotator. The antibody was recovered by addition of Protein L-agarose-conjugated beads [2.5 % (v/v), Santa Cruz Biotechnology] followed by incubation for 3 h at 4 °C on a rotator. The beads were washed three times by centrifugation (60 s at 13 000 ***g***) and resuspended in solubilization buffer (60 μl). The samples were then diluted with NuPAGE SDS sample buffer (Invitrogen) supplemented with 100 mM DTT (dithiothreitol). Elution was performed by incubating the beads at 50 °C for 60 min followed by centrifugation (60 s at 13 000 ***g***). Aliquots (typically 10 μl) were subject to SDS/PAGE followed by Western blot analysis.

Sucrose-density-gradient centrifugation

Detergent-solubilized cell homogenates (200 μl) were layered on to 1.8 ml 5–20 % (w/v) sucrose density gradients (prepared in 3 % increments in solubilization buffer) and centrifuged in a swing-out rotor at 166 000 ***g*** for 3.5 h at 4 °C. Fractions (195 μl) were collected from the top of the gradient and aliquots (20 μl) were subject to SDS/PAGE followed by Western blot analysis. Gradients were calibrated by analysing the distribution of the following standards (2 mg/ml) run in parallel and detected using the BCA protein assay: cytochrome *c* (12 kDa), alcohol dehydrogenase (150 kDa), β-amylase (200 kDa) and apoferritin (443 kDa).

Gel filtration

Detergent-solubilized cell homogenates (200 μl) were injected on to a Superdex 200 HR 10/30 column linked to an

ÄKTA FPLC system (Amersham Biosciences) and equilibrated with solubilization buffer. Fractions (1 ml) were collected at a flow rate of 0.5 ml/min and concentrated by Microcon YM-10 centrifugal filter devices (Millipore) to ~60 μl. Equivalent volumes (typically 25 μl) were subjected to SDS/PAGE followed by Western blot analysis. The column was calibrated by analysing the elution of the following standards (10 mg/ml) detected by absorbance at 280 nm: alcohol dehydrogenase (150 kDa), β-amylase (200 kDa), apoferritin (443 kDa) and thyroglobulin (669 kDa).

Chemical cross-linking

HEK-293 cells expressing the specified Myc- or GFP-tagged constructs were resuspended in PBS adjusted to pH 8, sonicated and samples (15 μg) were incubated with the indicated concentration of BS^3 [bis(sulfosuccinimidyl) suberate; Thermo Scientific] in a total volume of 20 μl. Following incubation (10 min at 37 °C), the pH of the samples was adjusted to 7.2 by addition of Tris. Aliquots (2 μg) were subject to SDS/PAGE followed by Western blot analysis.

Other methods

PNGase F (peptide N-glycosidase F) treatment, SDS/PAGE and Western blot analysis were performed as described previously [44]. Samples were separated using the NuPAGE system (Invitrogen). Both primary (anti-Myc or anti-GFP) and secondary horseradish-peroxidase-conjugated secondary antibodies were used at a 1:1000 dilution. Immunocytochemistry was also performed as described in [44] using Triton X-100-permeabilized cells, an anti-Myc primary antibody (1:100 dilution) and an Alexa Fluor® 568-conjugated secondary antibody (1:100 dilution), except that slides were stained with DAPI (4′,6-diamidino-2-phenylindole) prior to mounting.

RESULTS AND DISCUSSION

To probe the assembly of TPCs, we analysed the 25 constructs schematically depicted in Figure 1. All constructs were tagged at their C-termini with Myc tags or GFP (see the Materials and methods section). In the first set of experiments, we determined whether each hydrophobic domain of the TPC is capable of inserting into the membrane in isolation. To achieve this we performed Western blot analysis of membrane and soluble fractions prepared from cells expressing Myc-tagged domain I and II. We also analysed the connecting loop. As shown in Figure 2(A), domain I of TPC1 (encoded by $TPC1^{1–347}$–Myc) readily inserted into the membrane since the majority of the expressed protein appeared in the pellet fraction upon high-speed centrifugation. Essentially similar results were obtained using cells expressing domain II encoded by $TPC1^{427–816}$–Myc (Figure 2A). Notably, multiple bands were observed for domain II in pellet fractions that were sensitive to PNGase F, which removes carbohydrate residues from asparagine (Supplementary Figure S1A at http://www.BiochemJ.org/bj/441/bj4410317add.htm). These results indicate that domain II is N-glycosylated, as reported previously for full-length TPC1 [44]. Since N-glycosylation occurs within the luminal environment, these data provide further evidence for membrane insertion of domain II. Domain I and domain II of TPC2 encoded by $TPC2^{1–339}$ and $TPC2^{422–752}$ respectively were also found to readily insert into the membrane (Figure 2B). Similar to TPC1, domain II of TPC2 migrated as a heterogeneous population (Figure 2B). In contrast, the connecting loop of TPC1 encoded by $TPC1^{348–426}$–Myc was recovered in the supernatant fraction (Figure 2A). These data, summarized in Figures 2(C) and 2(D), indicate that each hydrophobic domain is capable of independently inserting into the membrane. Accordingly, immunocytochemical analysis of domain I and II of TPC1 showed a non-uniform perinuclear distribution, whereas the connecting loop was distributed evenly throughout the cytosol (Supplementary Figure S1B).

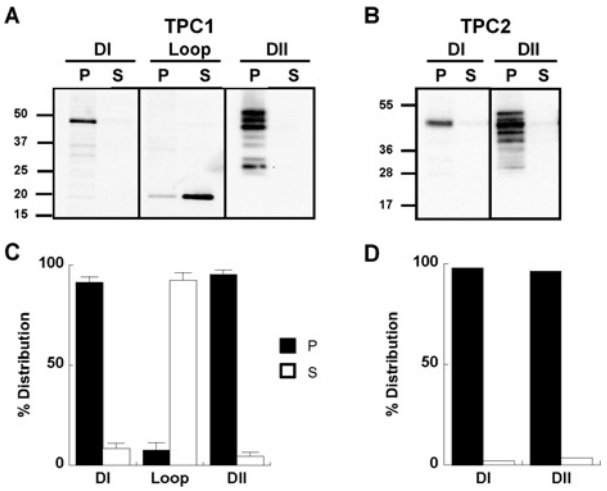

Figure 2 Membrane insertion of TPC domains

(**A** and **B**) Western blot analysis, using an anti-Myc antibody, of pellet (P) and supernatant (S) fractions prepared from cells expressing the indicated region of TPC1 (**A**) and TPC2 (**B**). The molecular mass in kDa is indicated on the left-hand side. Summary data quantifying the distribution of the expressed protein is shown in (**C**) ($n>3$) and (**D**) ($n=2$). DI, domain I; DII, domain II.

To determine how the individual hydrophobic domains of TPCs insert into the membrane, we focused on domain I of TPC1. We analysed constructs encoding the first two TM regions ($TPC1^{1–166}$–Myc), TM regions 3 and 4 ($TPC1^{167–225}$–Myc) and TM regions 5 and 6 ($TPC1^{226–347}$–Myc; Figure 1). Fractionation experiments similar to those described above revealed that a significant proportion of each construct was recovered in the pellet fraction (Figure 3A). These data suggest that TM regions 1, 3 and 5 all possess signal anchor activity, consistent with sequential co-translational integration of each TM region typical of other polytopic membrane proteins [46]. We noted, however, that insertion of TM 1 and 2 was less efficient than the other TM region pairs (summarized in Figure 3C). To further investigate this, we performed experiments where cell homogenates were incubated in the presence of Na_2CO_3 prior to fractionation. This treatment strips membranes of loosely associated proteins that fail to fully integrate into the membrane. As shown in Figure 3(B), Na_2CO_3 treatment had a modest effect on insertion of TM 3 and 4 and TM 5 and 6. Thus after treatment the majority of the protein was retained within the membrane (summarized in Figure 3D). However, a majority of TM 1 and 2 was recovered in the supernatant fraction in the presence of Na_2CO_3 (Figures 3B and 3D). These data further suggest that integration of the first two TM regions is inefficient. We note the presence of charged residues in TM regions 1 and 2 of both TPC1 and TPC2 (Figure 3E) which may inhibit translocation of the nascent polypeptide chain, as reported previously for cystic fibrosis transmembrane conductance regulator [47]. Alternatively, the TM regions may require stabilization by other regions within the domain. In voltage-gated K^+ channels, negatively charged residues in the second TM region interact with positively

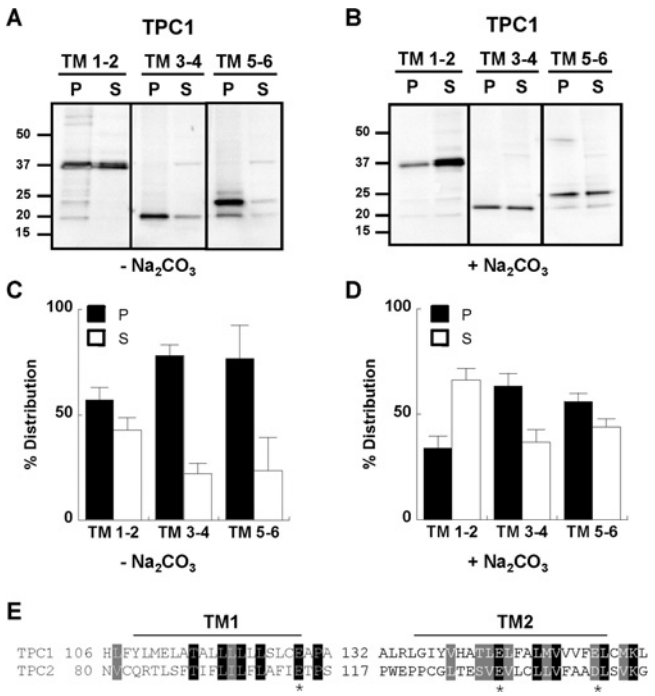

Figure 3 Membrane insertion of TM pairs

Western blot analysis, using an anti-Myc antibody, of pellet (P) and supernatant (S) fractions prepared from cells expressing the indicated pair of TM regions within domain I of TPC1. Fractionation was performed in the absence (**A**) or presence (**B**) of 0.1 M Na_2CO_3. The molecular mass in kDa is indicated on the left-hand side. (**C** and **D**) Summary data quantifying the distribution of the expressed protein ($n>3$). (**E**) Sequence alignment of TM regions 1 and 2 of TPC1 and TPC2 highlighting the presence of conserved charged residues (indicated by *).

charged residues in the fourth TM region to promote channel maturation [48–50]. Thus biogenesis of TPCs might proceed by both co- and 'post'-translational insertion of TM regions.

Previous studies have shown co-immunoprecipitation of heterologously expressed Myc- and GFP-tagged mouse TPC2 [26], indicating that TPCs probably form oligomers. Similar results were obtained with Myc- and GFP-tagged human TPC1 and TPC2 (results not shown). To identify the molecular determinants of the interaction, we analysed extracts from cells co-expressing GFP and Myc-tagged fragments of TPC1 and TPC2. When cell extracts expressing GFP- and Myc-tagged domain I were immunoprecipitated with an anti-Myc antibody and the immunopreciptates were probed with an anti-GFP antibody, we detected the presence of domain I–GFP ($TPC1^{1–347}$–GFP) by Western blot analysis (Figure 4A). These results indicate that domain I alone is capable of oligomerization. Domain II, which we showed above to insert independently into membranes, was also capable of oligomerization as evidenced by the co-immunoprecipitation of $TPC1^{427–816}$–GFP and $TPC1^{427–816}$–Myc (Figure 4A). Similar experiments using control IgG in place of the Myc antibody during immunoprecipitation failed to reveal an interaction (results not shown). GFP-tagged domain I and II of TPC2 ($TPC2^{1–339}$–GFP and $TPC2^{422–752}$–GFP) were also found to co-immunoprecipitate with the corresponding Myc-tagged construct (Figure 4A). In contrast, we detected only a weak interaction between Myc and GFP ($TPC1^{348–426}$–GFP)-tagged constructs encoding the connecting loop of TPC1 (Figure 4A), attesting to specificity. This was despite similar expression levels of all constructs (Figure 4A). These data indicate that both hydrophobic domains contribute to oligomerization in the channel complex.

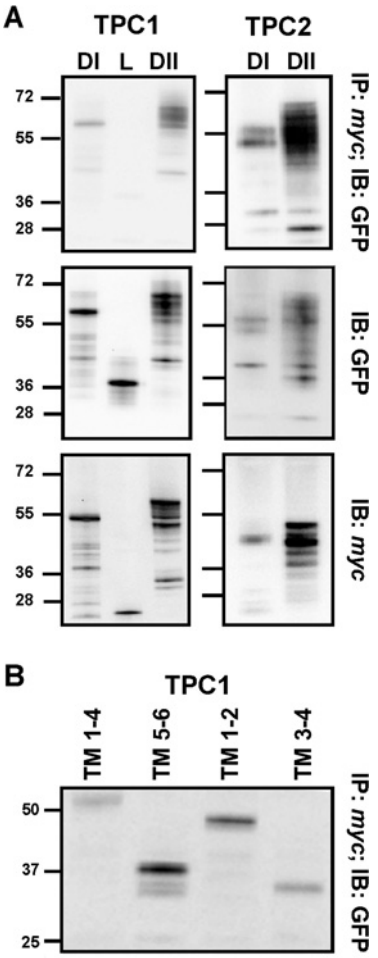

Figure 4 Oligomerization of TPCs

(**A**) Top panels: Western blot analysis using an anti-GFP antibody of immunoprecipitates prepared using an anti-Myc antibody from cells co-expressing GFP- and Myc-tagged domain I (DI), loop (L) or domain II (DII) of the indicated isoform. Western blot analysis using an anti-GFP or anti-Myc antibody of the detergent extracts prior to immunoprecipitation are shown in the middle and bottom panels respectively. (**B**) Western blot analysis using an anti-GFP antibody of immunoprecipitates prepared using an anti-Myc antibody from cells co-expressing the indicated GFP- and Myc-tagged TM regions of TPC1. Data are representative of 2–11 experiments. The molecular mass in kDa is indicated on the left-hand side. IB, immunoblot; IP, immunoprecipitation.

To further define interacting regions within TPCs, we again focused on domain I of TPC1. Ancestral voltage-gated ion channels were probable oligomeric complexes formed by subunits resembling TM regions 5 and 6, similar to extant K^+ leak channels [43]. We therefore analysed Myc- and GFP-tagged constructs corresponding to the first four TM regions ($TPC1^{1–225}$) and TM regions 5 and 6 ($TPC1^{226–347}$) of domain I (Figure 1). Co-immunoprecipitation experiments showed that Myc- and GFP-tagged TM 1–4 interacted (Figure 4B). These data indicate that TM regions 5 and 6 are not necessary for oligomerization of domain I. However, Myc- and GFP-tagged TM 5 and 6 also co-immunoprecipitated (Figure 4B). Similar results were obtained with TM 1 and 2 and TM 3 and 4 (Figure 4B). Thus any pair of TM regions within the first domain is capable of interaction. There is therefore marked redundancy at both the intra- and inter-domain levels in the molecular determinants that govern oligomerization of TPCs.

Table 1 Summary of domain cross-linking experiments

The size of the monomeric and dimeric sized bands and the ratio (dimer/monomer) is shown for each domain construct analysed. Results are means ± S.E.M. from *n* experiments.

Isoform	Domain	Construct	Monomeric size (kDa)	Dimeric size (kDa)	Ratio	*n*
TPC1	Domain I	$TPC1^{1–347}$–GFP	66 ± 1	138 ± 4	2.1 ± 0.07	7
TPC1	Domain II	$TPC1^{427–816}$–GFP	70 ± 1	156 ± 5	2.2 ± 0.06	4
TPC2	Domain I	$TPC2^{1–339}$–GFP	54 ± 2	125 ± 2	2.3 ± 0.07	3
TPC2	Domain II	$TPC2^{422–752}$–GFP	57 ± 2	126 ± 2	2.2 ± 0.05	3

Given that TPCs correspond to essentially one half of voltage-sensitive Ca^{2+} and Na^+ channels, TPCs are likely to form dimers. To gain insight into the domain architecture of the TPC complex we performed cross-linking of the individual hydrophobic domains using the lysine-reactive reagent BS^3. Western blot analysis of cell extracts expressing GFP-tagged domain I of TPC1 showed that BS^3-induced a clear concentration-dependent accumulation of protein that had a molecular mass approximately twice that in the absence of cross-linker (Table 1). Similar results were obtained using cell extracts expressing GFP-tagged domain II of TPC1 (Figure 5A and Table 1). These results suggest that individual domains can form dimers. Evidence for dimer formation upon cross-linking was also obtained for domain I and domain II of TPC2 (Figure 5B and Table 1). We noted the presence of domain dimers in the absence of cross-linker. Intriguingly this was isoform-specific, observable only for domain II of TPC1 and domain I of TPC2, and particularly notable for the latter. These data are suggestive of differences in the molecular make-up of TPC1 and TPC2.

It is notable that no tetrameric species were observed in the above experiments, given the tetrameric assembly of one-domain channels such as K^+ channels and TRP channels to which the TPC domains analysed in the present study are analogous. To investigate this further, we performed cross-linking of the first four TM regions ($TPC1^{1–225}$), and TM regions 5 and 6 ($TPC1^{226–347}$) of TPC1. As shown in Figure 5(C), TPC1 TM 1–4 formed dimers in the presence of cross-linker similar to domain I. In contrast, TM 5 and 6 formed both dimers and tetramers (Figure 5C). These data suggest a 'dimer of dimers' arrangement of the first four TM regions where contacts are formed with only one adjacent domain within the full-length dimer of TPCs. In contrast, the central pore is probably formed by interaction between all four pore loops in TM regions 5 and 6 (two from each subunit) (Figure 5D). Results of cross-linking, gel filtration and sucrose-density-gradient centrifugation of full-length TPCs in order to determine native size were equivocal. Thus whereas high molecular mass complexes (>400 kDa) were observed upon cross-linking and gel filtration, TPCs appeared much lighter (~150 kDa) on sucrose density gradients (Supplementary Figure S2 at http://www.BiochemJ.org/bj/441/bj4410317add.htm). Anomalous migration of TPCs is consistent with anomalous migration of endogenous NAADP receptors (detected by radioligand binding) in sea urchin eggs [51].

To conclude, we show that each hydrophobic domain of TPCs is capable of insertion and forming oligomers, probably reflective of the ancestral one-repeat channel from which it evolved. Between TM pairs within a domain, we identify co-operativity during insertion and redundancy during oligomerization. We also present evidence that TPCs probably form dimers involving differential interactions between and within individual domains. The results of the present study provide the first insight into the biogenesis of the TPCs.

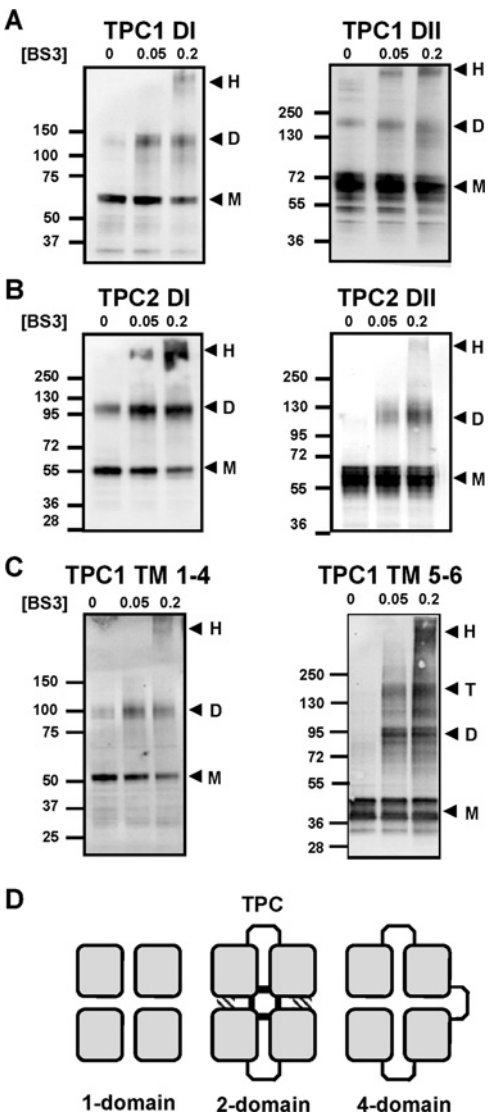

Figure 5 Cross-linking of TPCs

(**A**–**C**) Western blot analysis of GFP-tagged hydrophobic domains of TPC1 (**A**), TPC2 (**B**) or the indicated TM regions of TPC1 (**C**). Experiments were performed in the presence of the indicated concentration (in mM) of BS^3. The presence of monomeric (M), dimeric (D), tetrameric (T) or high-molecular-mass (H) products are highlighted by the arrows. The molecular mass in kDa is indicated on the left-hand side. (**D**) Schematic diagram showing the conservation of the four-domain (squares) architecture between tetrameric one-domain channels (e.g. K_v), dimeric two-domain channels (TPC) and monomeric four-domain channels (e.g. Ca_v). In TPCs, the central pore is likely to be formed by contacts between all four domains within the dimer (shaded regions), whereas regions outside the pore may form contacts with only one neighbouring domain (hatched regions).

AUTHOR CONTRIBUTION

Dev Churamani and Robert Hooper designed, performed and analysed experiments. Eugen Brailoiu assisted in the design of experiments. Sandip Patel directed the project and wrote the paper.

ACKNOWLEDGEMENT

We thank Chi Li for useful discussions.

FUNDING

This work was supported by the Biotechnology and Biological Sciences Research Council [grant number BB/G013721/1].

REFERENCES

1 Lee, H. C. (2001) Physiological functions of cyclic ADP-ribose and NAADP as calcium messengers. Annu. Rev. Pharmacol. Toxicol. **41**, 317–345
2 Patel, S., Churchill, G. C. and Galione, A. (2001) Coordination of Ca^{2+} signalling by NAADP. Trends Biochem. Sci. **26**, 482–489
3 Patel, S. (2004) NAADP-induced Ca^{2+} release: a new signaling pathway. Biol. Cell **96**, 19–28
4 Guse, A. H. and Lee, H. C. (2008) NAADP: a universal Ca^{2+} trigger. Sci. Signaling **1**, re10
5 Yamasaki, M., Masgrau, R., Morgan, A. J., Churchill, G. C., Patel, S., Ashcroft, S. J. H. and Galione, A. (2004) Organelle selection determines agonist-specific Ca^{2+} signals in pancreatic acinar and beta cells. J. Biol. Chem. **279**, 7234–7240
6 Pandey, V., Chuang, C. C., Lewis, A. M., Aley, P., Brailoiu, E., Dun, N., Churchill, G. C. and Patel, S. (2009) Recruitment of NAADP-sensitive acidic Ca^{2+} stores by glutamate. Biochem. J. **422**, 503–512
7 Galione, A., Morgan, A. J., Arredouani, A., Davis, L. C., Rietdorf, K., Ruas, M. and Parrington, J. (2010) NAADP as an intracellular messenger regulating lysosomal calcium-release channels. Biochem. Soc. Trans. **38**, 1424–1431
8 Lim, D., Kyozuka, K., Gragnaniello, G., Carafoli, E. and Santella, L. (2001) $NAADP^+$ initiates the Ca^{2+} response during fertilization of starfish oocytes. FASEB J. **15**, 2257–2267
9 Churchill, G. C., O'Neil, J. S., Masgrau, R., Patel, S., Thomas, J. M., Genazzani, A. A. and Galione, A. (2003) Sperm deliver a new messenger: NAADP. Curr. Biol. **13**, 125–128
10 Brailoiu, G. C., Gurzu, B., Gao, X., Parkesh, R., Aley, P. K., Trifa, D. I., Galione, A., Dun, N. J., Madesh, M., Patel, S. et al. (2010) Acidic NAADP-sensitive calcium stores in the endothelium: agonist-specific recruitment and role in regulating blood pressure. J. Biol. Chem. **285**, 37133–37137
11 Hooper, R. and Patel, S. (2012) NAADP on target. Adv. Exp. Med. Biol., in the press
12 Cordiglieri, C., Odoardi, F., Zhang, B., Nebel, M., Kawakami, N., Klinkert, W. E., Lodygin, D., Luhder, F., Breunig, E., Schild, D. et al. (2010) Nicotinic acid adenine dinucleotide phosphate-mediated calcium signalling in effector T cells regulates autoimmunity of the central nervous system. Brain **133**, 1930–1943
13 Churchill, G. C., Okada, Y., Thomas, J. M., Genazzani, A. A., Patel, S. and Galione, A. (2002) NAADP mobilizes Ca^{2+} from reserve granules, lysosome-related organelles, in sea urchin eggs. Cell **111**, 703–708
14 Mitchell, K. J., Lai, F. A. and Rutter, G. A. (2003) Ryanodine receptor type I and nicotinic acid adenine dinucleotide phosphate (NAADP) receptors mediate Ca^{2+} release from insulin-containing vesicles in living pancreatic β cells (MIN6). J. Biol. Chem. **278**, 11057–11064
15 Menteyne, A., Burdakov, A., Charpentier, G., Petersen, O. H. and Cancela, J. M. (2006) Generation of specific Ca^{2+} signals from Ca^{2+} stores and endocytosis by differential coupling to messengers. Curr. Biol. **16**, 1931–1937
16 Patel, S. and Docampo, R. (2010) Acidic calcium stores open for business: expanding the potential for intracellular Ca^{2+} signaling. Trends Cell Biol. **20**, 277–286
17 Patel, S. and Muallem, S. (2011) Acidic Ca^{2+} stores come to the fore. Cell Calcium **50**, 109–112
18 Cancela, J. M., Churchill, G. C. and Galione, A. (1999) Coordination of agonist-induced Ca^{2+}-signalling patterns by NAADP in pancreatic acinar cells. Nature **398**, 74–76
19 Gerasimenko, J. V., Maruyama, Y., Yano, K., Dolman, N., Tepikin, A. V., Petersen, O. H. and Gerasimenko, O. V. (2003) NAADP mobilizes Ca^{2+} from a thapsigargin-sensitive store in the nuclear envelope by activating ryanodine receptors. J. Cell Biol. **163**, 271–282
20 Dammermann, W., Zhang, B., Nebel, M., Cordiglieri, C., Odoardi, F., Kirchberger, T., Kawakami, N., Dowden, J., Schmid, F., Dornmair, K. et al. (2009) NAADP-mediated Ca^{2+} signaling via type 1 ryanodine receptor in T cells revealed by a synthetic NAADP antagonist. Proc. Natl. Acad. Sci. U.S.A. **106**, 10678–10683
21 Moccia, F., Lim, D., Nusco, G. A., Ercolano, E. and Santella, L. (2003) NAADP activates a Ca^{2+} current that is dependent on F-actin cytoskeleton. FASEB J. **13**, 1907–1909
22 Beck, A., Kolisek, M., Bagley, L. A., Fleig, A. and Penner, R. (2006) Nicotinic acid adenine dinucleotide phosphate and cyclic ADP-ribose regulate TRPM2 channels in T lymphocytes. FASEB J. **20**, 962–964
23 Guse, A. H. (2009) Second messenger signaling: multiple receptors for NAADP. Curr. Biol. **19**, R521–R523
24 Brailoiu, E., Churamani, D., Cai, X., Schrlau, M. G., Brailoiu, G. C., Gao, X., Hooper, R., Boulware, M. J., Dun, N. J., Marchant, J. S. and Patel, S. (2009) Essential requirement for two-pore channel 1 in NAADP-mediated calcium signaling. J. Cell Biol. **186**, 201–209
25 Calcraft, P. J., Ruas, M., Pan, Z., Cheng, X., Arredouani, A., Hao, X., Tang, J., Rietdorf, K., Teboul, L., Chuang, K. T. et al. (2009) NAADP mobilizes calcium from acidic organelles through two-pore channels. Nature **459**, 596–600
26 Zong, X., Schieder, M., Cuny, H., Fenske, S., Gruner, C., Rotzer, K., Griesbeck, O., Harz, H., Biel, M. and Wahl-Schott, C. (2009) The two-pore channel TPCN2 mediates NAADP-dependent Ca^{2+}-release from lysosomal stores. Pflügers Arch. **458**, 891–899
27 Brailoiu, E., Hooper, R., Cai, X., Brailoiu, G. C., Keebler, M. V., Dun, N. J., Marchant, J. S. and Patel, S. (2010) An ancestral deuterostome family of two-pore channels mediate nicotinic acid adenine dinucleotide phosphate-dependent calcium release from acidic organelles. J. Biol. Chem. **285**, 2897–2901
28 Ruas, M., Rietdorf, K., Arredouani, A., Davis, L. C., Lloyd-Evans, E., Koegel, H., Funnell, T. M., Morgan, A. J., Ward, J. A., Watanabe, K. et al. (2010) Purified TPC isoforms form NAADP receptors with distinct roles for Ca^{2+} signaling and endolysosomal trafficking. Curr. Biol. **20**, 703–709
29 Lee, H. C. and Aarhus, R. (1995) A derivative of NADP mobilizes calcium stores insensitive to inositol trisphosphate and cyclic ADP-ribose. J. Biol. Chem. **270**, 2152–2157
30 Cai, X. and Patel, S. (2010) Degeneration of an intracellular ion channel in the primate lineage by relaxation of selective constraints. Mol. Biol. Evol. **27**, 2352–2359
31 Ogunbayo, O. A., Zhu, Y., Rossi, D., Sorrentino, V., Ma, J., Zhu, M. X. and Evans, A. M. (2011) cADPR activates ryanodine receptors while NAADP activates two pore domain channels. J. Biol. Chem. **286**, 9136–9140
32 Pereira, G. J., Hirata, H., Fimia, G. M., do Carmo, L. G., Bincoletto, C., Han, S. W., Stilhano, R. S., Ureshino, R. P., Bloor-Young, D., Churchill, G. et al. (2011) Nicotinic acid adenine dinucleotide phosphate (NAADP) regulates autophagy in cultured astrocytes. J. Biol. Chem. **286**, 27875–27881
33 Dionisio, N., Albarran, L., Lopez, J. J., Berna-Erro, A., Salido, G. M., Bobe, R. and Rosado, J. A. (2011) Acidic NAADP-releasable Ca^{2+} compartments in the megakaryoblastic cell line MEG01. Biochim. Biophys. Acta **1813**, 1483–1494
34 Brailoiu, E., Rahman, T., Churamani, D., Prole, D. L., Brailoiu, G. C., Hooper, R., Taylor, C. W. and Patel, S. (2010) An NAADP-gated two-pore channel targeted to the plasma membrane uncouples triggering from amplifying Ca^{2+} signals. J. Biol. Chem. **285**, 38511–38516
35 Schieder, M., Rotzer, K., Bruggemann, A., Biel, M. and Wahl-Schott, C. A. (2010) Characterization of two-pore channel 2 (TPCN2)-mediated Ca^{2+} currents in isolated lysosomes. J. Biol. Chem. **285**, 21219–21222
36 Pitt, S. J., Funnell, T., Sitsapesan, M., Venturi, E., Rietdorf, K., Ruas, M., Ganesan, A., Gosain, R., Churchill, G. C., Zhu, M. X. et al. (2010) TPC2 is a novel NAADP-sensitive Ca^{2+}-release channel, operating as a dual sensor of luminal pH and Ca^{2+}. J. Biol. Chem. **285**, 24925–24932
37 Tugba Durlu-Kandilci, N., Ruas, M., Chuang, K. T., Brading, A., Parrington, J. and Galione, A. (2010) TPC2 proteins mediate nicotinic acid adenine dinucleotide phosphate (NAADP)- and agonist-evoked contractions of smooth muscle. J. Biol. Chem. **285**, 24925–24932
38 Aley, P. K., Mikolajczyk, A. M., Munz, B., Churchill, G. C., Galione, A. and Berger, F. (2010) Nicotinic acid adenine dinucleotide phosphate regulates skeletal muscle differentiation via action at two-pore channels. Proc. Natl. Acad. Sci. U.S.A. **107**, 19927–19932
39 Esposito, B., Gambara, G., Lewis, A. M., Palombi, F., D'Alessio, A., Taylor, L. X., Genazzani, A. A., Ziparo, E., Galione, A., Churchill, G. C. and Filippini, A. (2011) NAADP links histamine H1 receptors to secretion of von Willebrand factor in human endothelial cells. Blood **117**, 4968–4977
40 Boittin, F. X., Galione, A. and Evans, A. M. (2003) Nicotinic acid adenine dinucleotide phosphate mediates Ca^{2+} signals and contraction in arterial smooth muscle via a two-pool mechanism. Circ. Res. **91**, 1168–1175
41 Brailoiu, E., Churamani, D., Pandey, V., Brailoiu, G. C., Tuluc, F., Patel, S. and Dun, N. J. (2006) Messenger-specific role for NAADP in neuronal differentiation. J. Biol. Chem. **281**, 15923–15928
42 Patel, S., Marchant, J. S. and Brailoiu, E. (2010) Two-pore channels: regulation by NAADP and customized roles in triggering calcium signals. Cell Calcium **47**, 480–490
43 Yu, F. H., Yarov-Yarovoy, V., Gutman, G. A. and Catterall, W. A. (2005) Overview of molecular relationships in the voltage-gated ion channel superfamily. Pharmacol. Rev. **57**, 387–395

44 Hooper, R., Churamani, D., Brailoiu, E., Taylor, C. W. and Patel, S. (2011) Membrane topology of NAADP-sensitive two-pore channels and their regulation by N-linked glycosylation. J. Biol. Chem. **286**, 9141–9149
45 Yamaguchi, S., Jha, Y., Li, Q., Soyombo, A. A., Dickinson, G. D., Churamani, D., Brailoiu, E., Patel, S. and Muallem, S. (2011) Transient receptor potential mucolipin 1 (TRPML1) and two-pore channels are functionally independent organellar ion channels. J. Biol. Chem. **286**, 22934–22942
46 Skach, W. R. (2009) Cellular mechanisms of membrane protein folding. Nat. Struct. Mol. Biol. **16**, 606–612
47 Lu, Y., Xiong, X., Helm, A., Kimani, K., Bragin, A. and Skach, W. R. (1998) Co- and posttranslational translocation mechanisms direct cystic fibrosis transmembrane conductance regulator N terminus transmembrane assembly. J. Biol. Chem. **273**, 568–576

Received 8 September 2011/11 October 2011; accepted 12 October 2011
Published as BJ Immediate Publication 12 October 2011, doi:10.1042/BJ20111617

48 Papazian, D. M., Shao, X. M., Seoh, S. A., Mock, A. F., Huang, Y. and Wainstock, D. H. (1995) Electrostatic interactions of S4 voltage sensor in Shaker K^+ channel. Neuron **14**, 1293–1301
49 Tiwari-Woodruff, S. K., Schulteis, C. T., Mock, A. F. and Papazian, D. M. (1997) Electrostatic interactions between transmembrane segments mediate folding of Shaker K^+ channel subunits. Biophys. J. **72**, 1489–1500
50 Zhang, L., Sato, Y., Hessa, T., von Heijne, G., Lee, J. K., Kodama, I., Sakaguchi, M. and Uozumi, N. (2007) Contribution of hydrophobic and electrostatic interactions to the membrane integration of the Shaker K^+ channel voltage sensor domain. Proc. Natl. Acad. Sci. U.S.A. **104**, 8263–8268
51 Berridge, G., Dickinson, G., Parrington, J., Galione, A. and Patel, S. (2002) Solubilization of receptors for the novel Ca^{2+}-mobilizing messenger, nicotinic acid adenine dinucleotide phosphate. J. Biol. Chem. **277**, 43717–43723

Biochem. J. (2012) **441**, 317–323 (Printed in Great Britain) doi:10.1042/BJ20111617

SUPPLEMENTARY ONLINE DATA

Domain assembly of NAADP-gated two-pore channels

Dev CHURAMANI*[1], Robert HOOPER*[1], Eugen BRAILOIU† and Sandip PATEL*[2]

*Department of Cell and Developmental Biology, University College London, London WC1E 6BT, U.K., and †Department of Pharmacology, Temple University School of Medicine, Philadelphia, PA 19140, U.S.A.

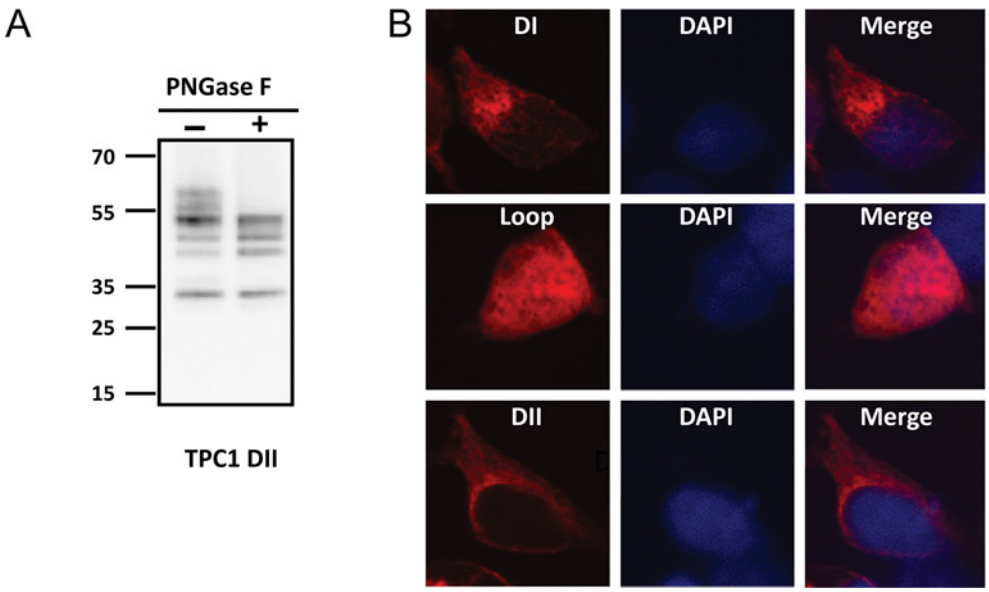

Figure S1 Membrane insertion of TPC domains

(**A**) Western blot analysis using an anti-Myc antibody of pellet fractions prepared from cells expressing domain II of TPC1 that were treated with (+) or without (−) PNGase F to remove carbohydrate residues. The molecular mass in kDa is indicated on the left-hand side. (**B**) Immunocytochemical analysis using an anti-Myc antibody of cells expressing the indicated domain of TPC1 (red). Staining of nuclei with DAPI (4′, 6-diamidino-2-phenylindole) is shown in blue and overlays of the images are on the right-hand side. DI, domain I; DII, domain II.

[1] These authors contributed equally to this work.
[2] To whom correspondence should be addressed (email patel.s@ucl.ac.uk).

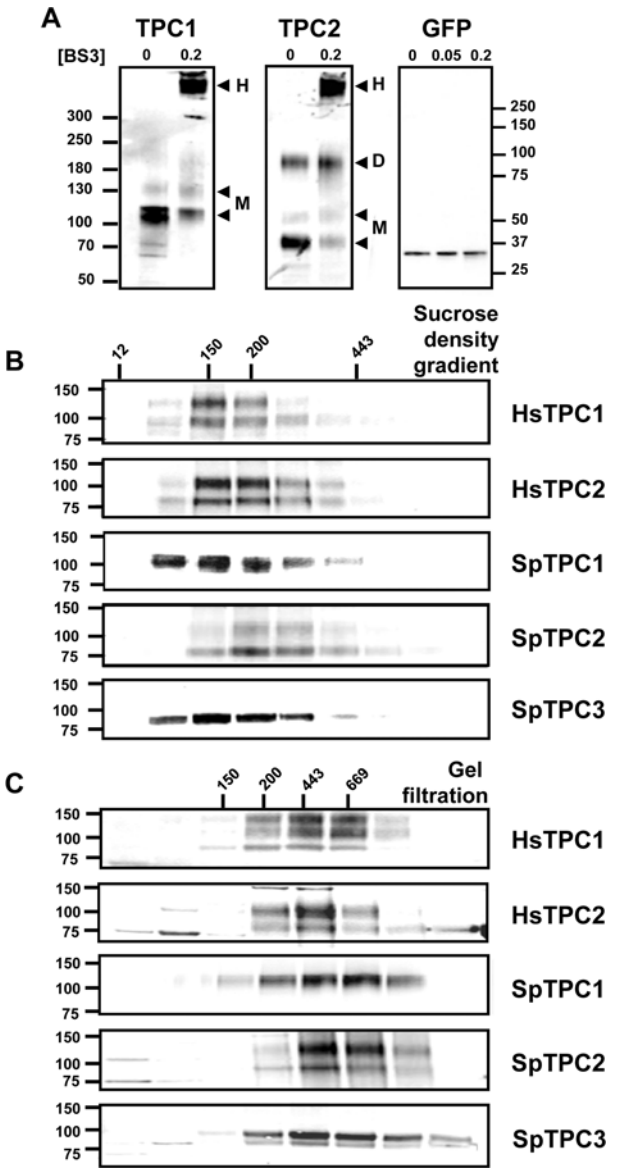

Figure S2 Native molecular mass of TPCs

(**A**) Western blot analysis of full-length Myc-tagged TPCs or GFP alone. Experiments were performed in the presence of the indicated concentration (in mM) of BS^3. The presence of monomeric (M), dimeric (D) or high molecular mass (H) products is highlighted by the arrows. (**B** and **C**) Western blot analysis of detergent extracts fractionated on either sucrose gradients (**B**) or a gel-filtration column (**C**). Extracts were prepared from cells expressing human (Hs) or sea urchin (Sp) TPCs. The migration of proteins of known size (in kDa) on the gradients or column are indicated horizontally. Data are representative of two to five experiments. The molecular mass in kDa is indicated on the left-hand side.

Table S1 Sequences of the forward and reverse oligonucleotide primers used for PCR amplification of TPC fragments

Construct	Direction	Oligonucleotide primer sequence (5′→3′)
$TPC1^{1–347}$	Forward	CACCATCGATATGGCTGTGAGTTTGGATGAC
	Reverse	CCTTGAATTCGAGCGGTAGGCATGCTGGATA
$TPC1^{348–426}$	Forward	CACCATCGATATGGCTCTGCTCATCAGCCAGAGGA
	Reverse	CCTTGAATTCGACGTCCTGGGAAGCTCATC
$TPC1^{427–816}$	Forward	CACCATCGATATGGCGCTCCTCATCTTCAAAG
	Reverse	CCTTGAATTCGAGGTAACGGTCTGGGAGCG
$TPC1^{1–166}$	Forward	CACCATCGATATGGCTGTGAGTTTGGATGAC
	Reverse	CCTTGAATTCGAGGTGTGGAGGCCCAGC
$TPC1^{167–225}$	Forward	CACCATCGATATGGCTTTCATCCGGCACAAGC
	Reverse	CCTTGAATTCGAGATCTGCCGCAGGTTGCG
$TPC1^{226–347}$	Forward	CACCATCGATATGGCTTTCCAGTCCCTGCCGC
	Reverse	CCTTGAATTCGAGCGGTAGGCATGCTGGATA
$TPC1^{1–225}$	Forward	CACCATCGATATGGCTGTGAGTTTGGATGACGAC
	Reverse	CCTTGAATTCGAGATCTGCCGCAGGTTGCG
$TPC2^{1–339}$	Forward	CACCGAATTCATGGCGGAACCCCAG
	Reverse	AGGCTCGAGTTCAAAGGCAGCCCGGGTTC
$TPC2^{422–752}$	Forward	CGCGAATTCATGGCGTTTCTGCAGAGCGCCCAG
	Reverse	AGGCTCGAGCCTGCACAGCCACAGGT

Received 8 September 2011/11 October 2011; accepted 12 October 2011
Published as BJ Immediate Publication 12 October 2011, doi:10.1042/BJ20111617